Nat.Lab. Unclassified Report UR 2000/825

Date of issue: 11/00

The drift region of high-voltage MOS devices

I.E.M. Severens

Unrestricted
©Philips Electronics 2000

Authors' address data: I.E.M. Severens; IEMSeverens@hotmail.com

©Philips Electronics N.V. 2000
All rights are reserved. Reproduction in whole or in part is
prohibited without the written consent of the copyright owner.

Unclassified Report: UR 2000/825

Title: The drift region of high-voltage MOS devices

Author(s): I.E.M. Severens

Reviewed by: A.C.T. Aarts

Part of project: Compact Modelling

Customer: Philips Semiconductors

Keywords: Semiconductor physics; LDMOS; modelling; high-voltage; drift region; transition region; MOS Model 31; pn-junction

Abstract: In this report a comparison between the transition region, where the current moves in radial direction, and the drift region, where the current moves parallel to the oxide, is made. Several analytic and numerical methods are derived to describe the potential and the current in both regions as function of the applied voltages and the geometry of the device.

Conclusions:

- The drift and transition region of LDMOS devices differ not only in geometry, but also in electrical behaviour.
- In the transition region the current is pinched-off at low values of the applied voltages.
- In the transition region the electric field is very high. Saturation of the current seems to happen at even very low applied voltages.

©Philips Electronics N.V. 2000

 ©Philips Electronics N.V. 2000

Contents

1 Introduction **1**

2 Problem formulation **1**

3 Depletion layers **2**

3.1 PN-junction 2

3.2 Oxide-silicon junction 4

4 Drift region **6**

4.1 Analytic solution 6

4.2 Numerical solution 9

5 Transition region **10**

5.1 Potential in depletion layer 11

5.2 Problem definition transition region 12

6 Potential in transition region **13**

6.1 First analytic approach 14

6.2 Analytic solution 17

6.3 First numerical approach 19

6.4 Numerical solution 19

7 Comparison **21**

7.1 Drift and transition region 22

7.2 Analytic and numerical method 23

8 Discussion **24**

9 Conclusions and recommendations **25**

A Numerical determination potential in drift region **27**

B Exact solution transition region **28**

C Numerical determination potential transition region. **29**

D Numerical method for characteristics **30**

©Philips Electronics N.V. 2000

E Fit of MM31 **31**

References **33**

Distribution

©Philips Electronics N.V. 2000

1 Introduction

An integrated circuit (IC) consists of many thousands of semiconductor devices (transistors). In practice, there is an urgent need for mathematical models of transistors, since such models allow to simulate the behaviour of an IC. The physics underlying a semiconductor is reasonably well understood and finite-element methods may be used for simulation. Finite-element methods, however, require a lot of computing time and memory. For a full IC with its many transistors a finite-element model per separate transistor is therefore not manageable. In circuit simulation programs, the electrical characteristics of IC components such as MOSFETs, bipolar transistors and interconnect lines are calculated using 'compact models'. A compact model is a physical model, describing currents, charges and noise of a device as a function of applied bias voltages, temperature and geometry. The physical parameters and geometrical dimensions are input to the model in the form of an electrical parameter set. The electrical parameters are determined from measurements.
The increased performance of integrated circuits is based upon the continuous reduction of transistor dimensions into the deep-submicron region. The industry is rapidly approaching the 100-nm barrier. Understanding the physical effects involved in scaling-down the feature size is essential for the efficient exploitation of these technologies.
In the following section we describe an LDMOS device, used for high voltages, in some detail and specify the parameters involved. The overall model of the device will be a combination of models for various regions in the device. We identify two such regions, the drift region and the transition region. In section 3 we will review the depletion and accumulation layers of these regions. The formulas derived in that section will be used throughout this report. In section 4 we will investigate the drift region. The transition region will be reviewed in detail in section 5 and 6. Finally, in section 7 and 8 a comparison between the electric behaviour of the drift and transition region will be made.

2 Problem formulation

In figure 1 a cross-section of an LDMOS device is shown. In the top part a strip of oxide separates two strips of metal called the *source* (on the left) and the *drain* (on the right). If we set a voltage $V_d - V_s > 0$ across the two metal strips, electrons will move from source to drain, and hence, an electrical current will flow from right to left. The current lines are depicted as dashed curves in figure 1. The current will flow in the white regions which contain silicon. In fact, all material below the strip of oxide is inhomogeneous silicon, where the inhomogenity is due to a variable amount of doping. In figure 1 the concentrations of doping are denoted by n^+ and n^- for respectively heavy and less heavy n-doped silicon, and p^+ and p^- for respectively heavy and less heavy p-doped silicon. Due to the externally applied gate voltage V_g and substrate voltage V_b, the free electrons either accumulate or diffuse at the surface of the n-type silicon and they diffuse across the pn-junctions. The diffusion results in *depletion layers*, where there are hardly any free electrons left.
In the device we identify a *drift* region, a large region in the center of the device, and a tiny *transition* region, below the gate (see figure 1). Their respective geometries differ a lot and as a result the models for them differ as well. For the drift region several compact models have been developed. One of these compact models is MOS model 31, see [1] and [2]. In this model the influence of the transition region isn't taken in account. Due to the continuous decrease of the dimensions of the transistors the influence of the transition region is becoming more and more important.

©Philips Electronics N.V. 2000

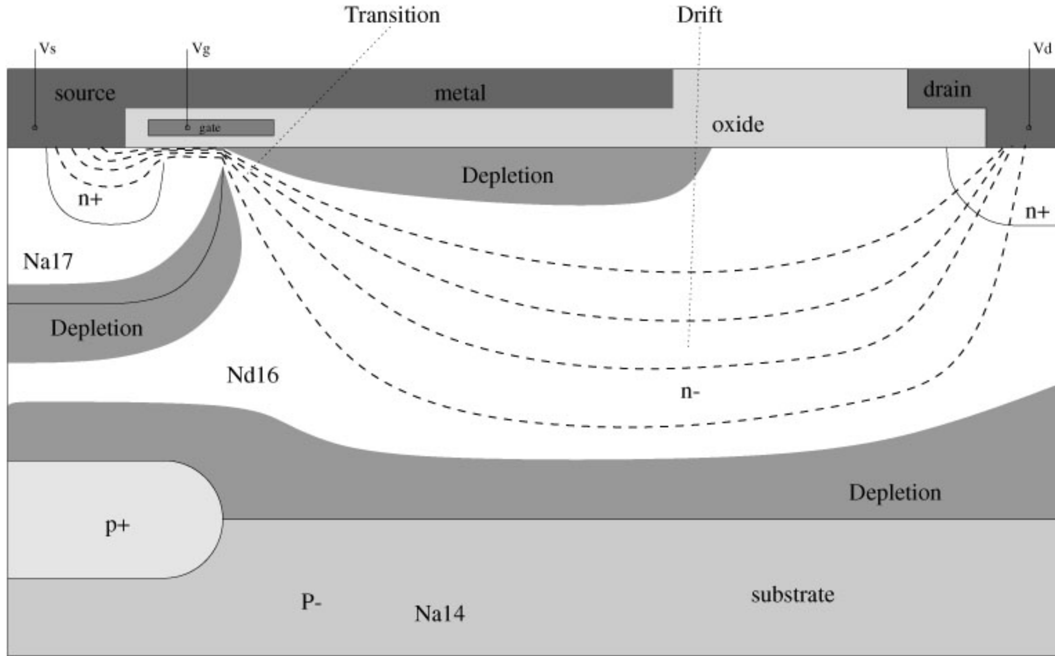

Figure 1: *Schematic representation of an LDMOS device.*

3 Depletion layers

As described in the previous section, depletion layers are formed at pn-junctions and oxide-silicon interfaces. In figure 1 these are the dark grey layers. They act as barriers through which only a negligible amount of current can flow. The size of the depletion layers depends on the voltages applied, so by changing the various voltages it is possible to shrink or enlarge the depletion layers, thereby modifying the shape of the channel through which current can flow. In our analysis we make use of the Maxwell equations, which simplify in the stationary case to

$$\nabla \cdot \mathbf{D} = \rho, \quad \nabla \times \mathbf{E} = \mathbf{0}, \quad \nabla \cdot \mathbf{J} = 0, \tag{3.1}$$

and the constitutive relations

$$\mathbf{D} = \varepsilon \mathbf{E}, \quad \mathbf{J} = -q\mu_n n \mathbf{E}, \quad \rho = q(p - n + N_d - N_a). \tag{3.2}$$

Here, $\mathbf{D}$ is the electric induction, $\mathbf{E}$ the electric field intensity, $\mathbf{J}$ the current density, ρ the charge density, μ_n the mobility of the electrons, n the free-electron concentration, p the hole concentration, q the electron charge, and ε the permittivity of the material. N_d is the doping concentration of n-type silicon (then $N_a = 0$) and N_a is the doping concentration of p-type silicon (then $N_d = 0$).

3.1 PN-junction

In this subsection we will review the depletion layer formed at a pn-junction. For simplicity we consider here the one-dimensional case of a p-material in the region $x < 0$ and an n-material in the region $x > 0$, see figure 2. In the p-type silicon there are more holes than free electrons, in the n-type silicon

 ©Philips Electronics N.V. 2000

it is the other way round. Because of this difference, electrons will diffuse from right to left in figure 2 across the junction, until a steady state is reached. This causes a positive charge in the n-type and a negative charge in the p-type silicon. We will assume that the length of the depletion region in the p, n-type silicon is l_2, l_1 respectively.

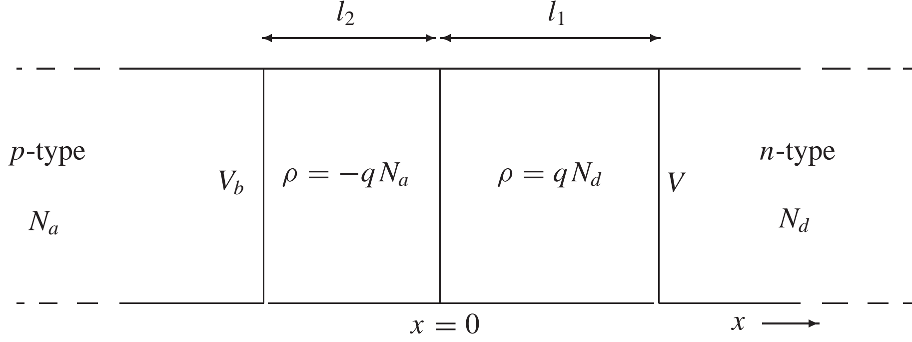

Figure 2: *Depletion region in pn-junction.*

We assume that at $x = l_1$ a voltage V is applied, whereas at $x = -l_2$ the voltage is kept at V_b. Because of $(3.1)^2$ we can introduce a potential φ according to

$$\mathbf{E} = -\nabla\varphi. \tag{3.3}$$

Evaluation of $(3.2)^3$ gives for the considered situation

$$\rho(x) = \begin{cases} 0, & x < -l_2, \\ -qN_a, & -l_2 < x < 0, \\ qN_d, & 0 < x < l_1, \\ 0, & x > l_1. \end{cases} \tag{3.4}$$

In the one-dimensional case the operator ∇ simplifies to d/dx, and $\mathbf{E} = E(x)\mathbf{e_x}$. Substitution of $(3.2)^1$ and (3.4) in $(3.1)^1$, and integration yields

$$E(x) = \begin{cases} c_1, & x < -l_2, \\ -\frac{qN_a}{\varepsilon}x + c_2, & -l_2 < x < 0, \\ \frac{qN_d}{\varepsilon}x + c_3, & 0 < x < l_1, \\ c_4, & x > l_1. \end{cases} \tag{3.5}$$

We can determine the constants $c1$, $c2$, $c3$ and $c4$ by applying the conditions $E(-\infty) = E(\infty) = 0$ and demanding continuity of E in $-l_2$, 0 and l_1. This gives

$$E(x) = \begin{cases} 0, & x < -l_2, \\ -\frac{qN_a}{\varepsilon}(x + l_2), & -l_2 < x < 0, \\ \frac{qN_d}{\varepsilon}(x - l_1), & 0 < x < l_1, \\ 0, & x > l_1, \end{cases} \tag{3.6}$$

and the condition $N_a l_2 = N_d l_1$, which implies electric neutrality of the pn-junction. Substitution of (3.6) in (3.3) and integration, taking in account that φ is continuous in $-l_2$, 0 and l_1 and $\varphi(-l_2) = V_b$, $\varphi(l_1) = V$, yields

$$l_2 = \sqrt{\frac{2\varepsilon N_d}{qN_a(N_a+N_d)}(V - V_b)}, \qquad l_1 = \sqrt{\frac{2\varepsilon N_a}{qN_d(N_a+N_d)}(V - V_b)}. \tag{3.7}$$

3.2 Oxide-silicon junction

In this subsection we will review the depletion layer at the interface of the oxide and the n-type silicon; see figure 1. We assume that there exists a parasitic charge Q_0 per unit area at the oxide-silicon interface. This parasitic charge is a uniform constant and is thus independent of the applied voltages. Due to the externally applied voltages, the free electrons either accumulate or diffuse at the surface of the n-type silicon. The diffusion or accumulation of electrons at the surface of the silicon results in a charge Q_g per unit area at the interface between the gate and the oxide, and in a charge Q_3 per unit area in the region $0 \leq y \leq l_3$; see figure 3.

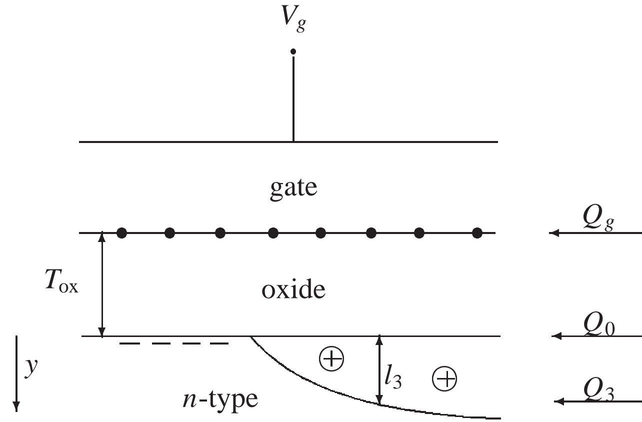

Figure 3: *Depletion and accumulation at the oxide-silicon interface.*

Accumulation occurs when the applied voltage V_g is such that electrons are attracted to the oxide-silicon interface. Diffusion on the other hand occurs when electrons are pushed away from the interface, resulting in a positive charge there. In case of accumulation, the region where the electrons accumulate is a very thin sheet below the oxide (i.e. $l_3 \approx 0$), and the charge Q_3 is negative. In case of diffusion, on the other hand, the region $0 \leq y \leq l_3$ has a certain thickness (i.e. $l_3 > 0$), and it has been depleted so that the charge Q_3 is positive. Electric neutrality of the material gives us

$$Q_g + Q_0 + Q_3 = 0, \tag{3.8}$$

where Q_3, in case of depletion, is given by

$$Q_3 = qN_d l_3. \tag{3.9}$$

We define φ_{ox} as the potential drop across the oxide, i.e $\varphi_{\text{ox}} = \varphi(-T_{\text{ox}}) - \varphi(0)$ and ϕ_{MS} as the contact potential between the gate and the n-type silicon. The total potential drop across the oxide layer is now given by

$$V_g - V^* = \varphi_{\text{ox}} + \phi_{MS}, \tag{3.10}$$

where V^* is defined as the potential at the oxide-silicon interface. By use of Gauss' law, the charge per unit area at the gate-oxide interface can be related to the potential drop across the oxide according to

$$Q_g = C_{\text{ox}}\varphi_{\text{ox}}, \tag{3.11}$$

 ©Philips Electronics N.V. 2000

where

$$C_{\text{ox}} = \frac{\varepsilon_{\text{ox}}}{T_{\text{ox}}} \tag{3.12}$$

represents the oxide capacitance per unit area. This yields

$$V^* = V_g - \frac{Q_g}{C_{\text{ox}}} - \phi_{MS}. \tag{3.13}$$

For simplicity we restrict ourselves to the one-dimensional case of a n-material in the region $y > 0$ against an oxide; see figure 4.

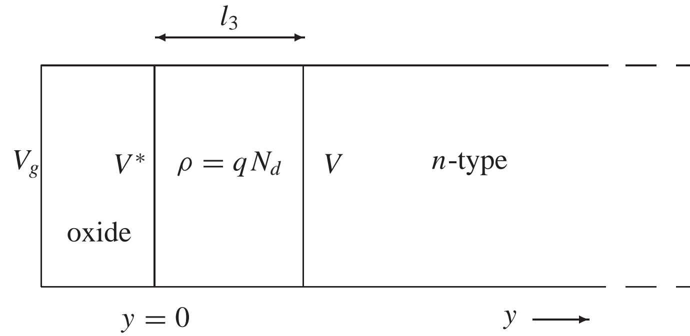

Figure 4: *One dimensional model for the depletion region at the oxide-silicon interface.*

The potential at the surface of the oxide is V^*, according to (3.13). We assume that the potential at $y = l_3$ is set at V. We define the so-called flat-band voltage V_{FB} as the voltage difference $V_g - V^*$ at which there is no charge at the surface of the n-type silicon, i.e $Q_3 = 0$. By use of (3.8), (3.11) and (3.13), the flat-band voltage is given by

$$V_{FB} = \phi_{MS} - \frac{Q_0}{C_{\text{ox}}}. \tag{3.14}$$

Because V_{FB} is generally small (at most 1V) compared to the applied voltages V_g and V_b, we take $V_{FB} = 0$. Evaluation of (3.2)[3] gives for the charge density in the silicon

$$\rho(x) = \begin{cases} qN_d, & 0 < y < l_3, \\ 0, & y > l_3. \end{cases} \tag{3.15}$$

Completely analogue to the previous subsection we derive that

$$l_3 = \sqrt{\frac{2\varepsilon}{qN_d}(V - V_g + \frac{Q_g}{C_{\text{ox}}} + \phi_{MS})}, \qquad V > V_g - \frac{Q_g}{C_{\text{ox}}} - \phi_{MS}. \tag{3.16}$$

If we substitute (3.16) into (3.8) and (3.9) and rearrange the terms, we obtain

$$\begin{aligned} \tfrac{C_{\text{ox}}}{2\varepsilon qN_d} 2\varepsilon qN_d(V - V_g + \tfrac{Q_g}{C_{\text{ox}}} + \phi_{MS}) \quad &+ \quad \sqrt{2\varepsilon qN_d(V - V_g + \tfrac{Q_g}{C_{\text{ox}}} + \phi_{MS})} + \\ &+ \quad Q_0 - C_{\text{ox}}(V - V_g - \phi_{MS}) = 0. \end{aligned} \tag{3.17}$$

©Philips Electronics N.V. 2000

We solve this equation with the *abc*-formula. This gives

$$
\begin{aligned}
l_3 &= \frac{\sqrt{2\varepsilon q N_d (V - V_g + \frac{Q_g}{C_{\text{ox}}} + \phi_{MS})}}{q N_d} \\
&= \frac{1}{qN_d} \frac{-1 + \sqrt{1 - 4\frac{C_{\text{ox}}}{2\varepsilon q N_d}(Q_0 - C_{\text{ox}}(V - V_g + \phi_{MS}))}}{2\frac{C_{\text{ox}}}{2\varepsilon q N_d}} \\
&= \frac{k_s}{qN_d}(\sqrt{V - V_g + V_{\text{Si}}} - \sqrt{V_{\text{Si}}}), \qquad V \geq V_g,
\end{aligned}
\tag{3.18}
$$

where V_{Si} and k_s are defined as

$$
V_{\text{Si}} = \frac{q\varepsilon N_d}{2C_{\text{ox}}^2}, \qquad k_s = \sqrt{2q\varepsilon N_d}. \tag{3.19}
$$

We still have to consider the situation that $V < V_g$. In that case accumulation will occur at the surface and Q_3 is a surface charge. In case of accumulation $l_3 \approx 0$ and the potential drop over the accumulation layer is zero, which implies that $V = V^*$. Substitution in (3.13) gives

$$
Q_g = -C_{\text{ox}}(V - V_g + \phi_{MS}). \tag{3.20}
$$

If we substitute (3.20) in (3.8) and set V_{FB} to zero, we get

$$
Q_3 = -C_{\text{ox}}(V_g - V), \qquad V < V_g. \tag{3.21}
$$

4 Drift region

For the long drift regions in DMOS-devices in 1994 a model, called MOS Model 30, was developed by Kloosterman [2]. Here we will use two different approaches to derive a model for long drift regions. These approaches will be of use to us in the development of a model for the transition region.

4.1 Analytic solution

In this subsection we will derive an analytic solution for the potential in the drift region. This analytic solution will be used to derive a formula for the current in the drift region. Consider the drift region in the n-type semiconductor material of the LDMOS device as sketched in figure 5. In the drift region we use the Carthesian coordinates x, y. We define V as the potential in the channel. The channel is bounded by two depletion layers. In the channel there is no net charge, i.e. $\rho = 0$. Substitution of (3.3), $(3.2)^1$ and $(3.2)^3$ in $(3.1)^1$ yields

$$
\Delta V = 0, \tag{4.1}
$$

in the channel. The potential at the source and drain of the drift region is set at V_s and V_d, so

$$
V(x_s, y) = V_s, \qquad V(x_d, y) = V_d. \tag{4.2}
$$

In the depletion layers only a negligible amount of current can flow, so no current will enter the depletion regions. Together with the Maxwell equations in integral form, the boundary conditions at the channel-depletion layers interface read

$$
\mathbf{E} \cdot \mathbf{n}|_{y=l_3(x)} = 0, \qquad \mathbf{E} \cdot \mathbf{n}|_{y=T_e - l_1(x)} = 0. \tag{4.3}
$$

 ©Philips Electronics N.V. 2000

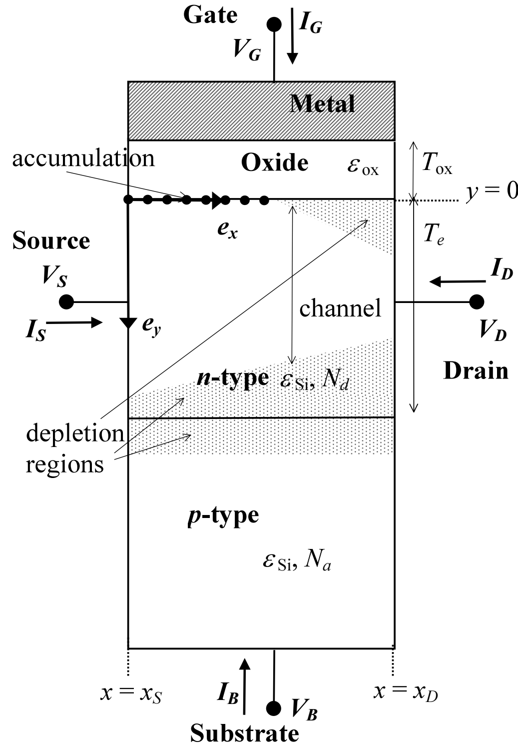

Figure 5: *Schematic representation of an LDMOS device.*

Here we have defined l_1 and l_3, according to the previous section, as the thickness of the depletion layer at the pn-junction and the oxide-silicon interface, respectively. At the oxide-silicon depletion layer the normal $\mathbf{n}$ is given by

$$\mathbf{n} = \frac{1}{\sqrt{(l_3'(x))^2 + 1}}(l_3'(x)\mathbf{e}_1 - \mathbf{e}_2), \tag{4.4}$$

whereas at the pn-junction the normal is given by

$$\mathbf{n} = \frac{1}{\sqrt{(l_1'(x))^2 + 1}}(l_1'(x)\mathbf{e}_1 + \mathbf{e}_2). \tag{4.5}$$

In order to derive an analytic solution for the potential we assume that $(V_d - V_s)/V_{\mathrm{Si}}$ is small, say δ. Summarising, we have the following problem

$$\begin{aligned}
&\Delta V = 0,\\
&V(x_s, y) = V_s,\\
&V(x_d, y) = V_s + V_{\mathrm{Si}}\delta,\\
&l_3'(x)\tfrac{\partial V}{\partial x}(x, l_3(x)) - \tfrac{\partial V}{\partial y}(x, l_3(x)) = 0,\\
&l_1'(x)\tfrac{\partial V}{\partial x}(x, T_e - l_1(x)) + \tfrac{\partial V}{\partial y}(x, T_e - l_1(x)) = 0,\\
&l_1(x) = \tfrac{k_b}{qN_d}\sqrt{V(x, T_e - l_1(x)) - V_b},\\
&l_3(x) = \tfrac{k_s}{qN_d}(\sqrt{V(x, l_1(x)) - V_g + V_{\mathrm{Si}}} - \sqrt{V_{\mathrm{Si}}}),
\end{aligned} \tag{4.6}$$

in which k_b is given by

$$k_b = \sqrt{2q\varepsilon_{\rm Si}\frac{N_a N_d}{N_a + N_d}}. \tag{4.7}$$

We assume that V, l_1 and l_3 can be written as

$$\begin{aligned} &V(x,y) = V_0(x,y) + V_1(x,y)\delta + ...,\\ &l_1(x) = l_{10}(x) + l_{11}(x)\delta + ...,\\ &l_3(x) = l_{30}(x) + l_{31}(x)\delta + ... \end{aligned} \tag{4.8}$$

Substitution of (4.8) in (4.6) gives for the zeroth order terms

$$\begin{aligned} &\Delta V_0 = 0,\\ &V_0(x_s, y) = V_s,\\ &V_0(x_d, y) = V_s,\\ &l'_{30}(x)\tfrac{\partial V_0}{\partial x}(x, l_{30}(x)) - \tfrac{\partial V_0}{\partial y}(x, l_{30}(x)) = 0,\\ &l'_{10}(x)\tfrac{\partial V_0}{\partial x}(x, T_e - l_{10}(x)) + \tfrac{\partial V_0}{\partial y}(x, T_e - l_{10}(x)) = 0,\\ &l_{10}(x) = \tfrac{k_b}{qN_d}\sqrt{V_0(x, T_e - l_{10}(x)) - V_b},\\ &l_{30}(x) = \tfrac{k_s}{qN_d}(\sqrt{V_0(x, l_{10}(x)) - V_g + V_{\rm Si}} - \sqrt{V_{\rm Si}}). \end{aligned} \tag{4.9}$$

The solution of (4.9) is $V_0 \equiv V_s$. This gives $l_{10}(x) \equiv l_{10}$ and $l_{30}(x) \equiv l_{30}$, where l_{10} and l_{30} are given by

$$l_{10} = \frac{k_b}{qN_d}\sqrt{V_s - V_b}, \qquad l_{30} = \frac{k_s}{qN_d}(\sqrt{V_s - V_g + V_{\rm Si}} - \sqrt{V_{\rm Si}}). \tag{4.10}$$

The problem for V_1 then simplifies to

$$\begin{aligned} &\Delta V_1 = 0,\\ &V_1(x_s, y) = 0,\\ &V_1(x_d, y) = V_{\rm Si},\\ &\tfrac{\partial V_1}{\partial y}(x, l_{30}(x)) = 0,\\ &\tfrac{\partial V_1}{\partial y}(x, T_e - l_{10}(x)) = 0, \end{aligned} \tag{4.11}$$

which has as solution

$$V_1(x,y) = \frac{x - x_s}{x_d - x_s}V_{\rm Si}. \tag{4.12}$$

Notice that $V_0(x,y) + \delta V_1(x,y)$ is a good approximation of the exact solution if $l'_1(x)$ and $l'_3(x)$ are small, i.e. $\frac{V_d - V_s}{x_d - x_s}$ is small. That is the case here, because we consider long channel drift regions. This gives for the electric field E_x(according to (3.3))

$$E_x = -\frac{V_d - V_s}{x_d - x_s}, \tag{4.13}$$

 ©Philips Electronics N.V. 2000

and consequently

$$J_x = qn\mu_n \frac{V_d - V_s}{x_d - x_s}. \tag{4.14}$$

Thus, for $V_d - V_s$ small, the electric field and current density are uniform. Here the free-electron concentration n is given by

$$n(x, y) = N_d - \frac{\rho(x, y)}{q}. \tag{4.15}$$

The total current I through the channel is now given by

$$\begin{aligned} I &= W \int_0^{T_e} J_x(x, y)dy \\ &= W\mu_n \frac{V_d - V_s}{x_d - x_s} \int_0^{T_e} qn(x, y)dy \\ &= W\mu_n \frac{V_d - V_s}{x_d - x_s}(qN_d T_e - Q_3 - Q_1), \end{aligned} \tag{4.16}$$

where W is the width of the device in z-direction. With (3.1)[3] the current I is uniform and constant, whereas the potential V is a function of x, and the charges Q_1 and Q_3 are a function of V and thus implicitly of x. Integration of (4.16) with respect to x from x_s to x_d, and division of the result by $x_d - x_s$ yields

$$I = W\mu_n \frac{V_d - V_s}{x_d - x_s}\left(qN_d T_e - \frac{1}{x_d - x_s}\int_{x_s}^{x_d} Q_3 dx - \frac{1}{x_d - x_s}\int_{x_s}^{x_d} Q_1 dx\right), \tag{4.17}$$

where

$$\begin{aligned} \int_{x_s}^{x_d} Q_3 dx &= \int_{x_s}^{x_d} k_s(\sqrt{V_0(x, l_3) + \delta V_1(x, l_3) - V_g + V_{\text{Si}}} - \sqrt{V_{\text{Si}}})dx \\ &= k_s(x_d - x_s)[\tfrac{2}{3}\tfrac{1}{V_d - V_s}\{(V_d - V_g + V_{\text{Si}})^{3/2} - (V_s - V_g + V_{\text{Si}})^{3/2}\} - \sqrt{V_{\text{Si}}}], \end{aligned} \tag{4.18}$$

and

$$\begin{aligned} \int_{x_s}^{x_d} Q_1 dx &= \int_{x_s}^{x_d} k_b\sqrt{V_0(x, T_e - l_1) + \delta V_1(x, T_e - l_1) - V_b}dx \\ &= \tfrac{2}{3}\tfrac{k_b(x_d - x_s)}{V_d - V_s}\{(V_d - V_b)^{3/2} - (V_s - V_b)^{3/2}\}. \end{aligned} \tag{4.19}$$

Here we have assumed that no accumulation occurs. Notice that this result is identical to the result in Aarts [1], page 18.

4.2 Numerical solution

In this subsection we will derive a numerical method to determine the potential in the channel. To that end we assume that the current through the drift region is known, say I. This constant and uniform current can for instance be obtained by experiments. Furthermore, we assume, as in the previous

subsection, that the current is only directed in the x-direction, so the potential only depends on x. This yields

$$J_x = q\mu_n n(x,y)\frac{dV(x)}{dx}. \tag{4.20}$$

Analogue to (4.16) we can derive that the total current I through the channel is now given by

$$I = W\mu_n \frac{dV(\xi)}{d\xi}(qN_dT_e - Q_3(V(\xi)) - Q_1(V(\xi))). \tag{4.21}$$

Integration of (4.21) with respect to ξ from x_s to x yields

$$\begin{aligned}\frac{(x-x_s)I}{W\mu} = \; & qN_dT_e(V(x)-V_s) - k_s[\tfrac{2}{3}\{(V(x)-V_g+V_{\text{Si}})^{3/2}+ \\ & -(V_s-V_g+V_{\text{Si}})^{3/2}\} - \sqrt{V_{\text{Si}}}(V(x)-V_s)]+ \\ & -\tfrac{2}{3}k_b[(V(x)-V_b)^{3/2}-(V_s-V_b)^{3/2}].\end{aligned} \tag{4.22}$$

From this expression we can determine $V(x)$ numerically for every x. We have done this with Mathematica, where we have used for the current I the expressions (4.17)-(4.19) derived in the previous subsection. For the program, see appendix A. The potential as a function of x can be seen in figure 6. Notice that the potential automatically fits the boundary conditions $V(x_s) = V_s$ and $V(x_d) = V_d$.

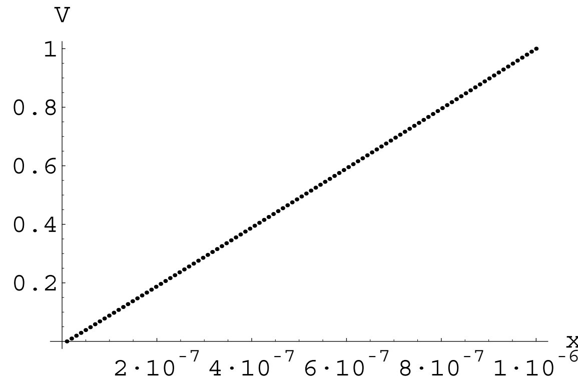

Figure 6: *Numerically determined potential $V(x)$ in drift region, $V_d = 1$V.*

Clearly we see the linear behaviour of the potential, as we derived in the previous subsection.

5 Transition region

The transition region is a small wedge-shaped region of about $2\mu\text{m}\times 2\mu\text{m}$ below the gate, as shown in figure 1. In the transition region we use the polar coordinates r, θ; see figure 7. The effective transition region G_t in the n-type silicon (i.e. the white region in figure 7) is bounded by two depletion layers. The first layer is formed underneath the oxide layer and runs from $\theta = 0$ to $\theta = \vartheta_s(r)$ (thus the thickness of that layer at radius r is $r \sin\vartheta_s(r)$, which should be compared to $l_3(x)$ for the drift region). The second layer runs from $\theta = \frac{\pi}{2} - \vartheta_1(r)$ to $\theta = \frac{\pi}{2}$ (thickness $r\sin\vartheta_1(r)$ comparable to $l_1(x)$). The deletion layer at the pn-junction in the n-type silicon extends into the p-type from $\theta = \frac{\pi}{2}$ to $\theta = \frac{\pi}{2} + \vartheta_2(r)$ (thickness $r\sin\vartheta_2(r)$ comparable to $l_2(x)$). As before, in these depletion layers $\mathbf{J} = \mathbf{0}$, and the charge density is qN_d in the ϑ_s -and ϑ_1-layer and $-qN_a$ in the ϑ_2-layer. We define V as the potential in the transition region G_t.

 ©Philips Electronics N.V. 2000

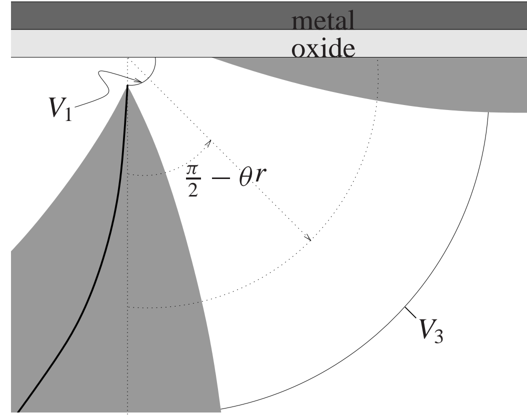

Figure 7: *The transition region.*

5.1 Potential in depletion layer

We will investigate the potential in the depletion layer

$$G_s = \{r, \theta | r_1 < r < r_3, 0 < \theta < \vartheta_s(r)\}. \tag{5.1}$$

The problem formulation for the potential $V_s = V_s(r, \theta)$ in G_s is given by

$$\begin{aligned} &\Delta V_s = -\tfrac{qN_d}{\varepsilon}, \\ &V_s(r, \vartheta_s(r)) = V(r, \vartheta_s(r)), \\ &V_s(r, 0) = V_g + \tfrac{qN_d r \sin \vartheta_s(r)}{C_{\text{ox}}}, \\ &V_s(r_1, \theta) = V_1(\theta), \\ &V_s(r_3, \theta) = V_3(\theta), \end{aligned} \tag{5.2}$$

where $\vartheta_s(r)$ is, according to (3.7)[1], given by

$$r \sin \vartheta_s(r) = \sqrt{\frac{2\varepsilon N_a}{qN_d(N_a + N_d)}(V(r, \vartheta_s(r)) - V_b)}. \tag{5.3}$$

The Δ operator is here defined as

$$\Delta = \frac{\partial^2}{\partial r^2} + \frac{1}{r}\frac{\partial}{\partial r} + \frac{1}{r^2}\frac{\partial^2}{\partial \theta^2}. \tag{5.4}$$

In the depletion layer, a thin-layer-approximation may be applied, implying that the Laplace operator Δ in the layers reduces to

$$\Delta = \frac{1}{r^2}\frac{\partial^2}{\partial \theta^2}. \tag{5.5}$$

This can be seen as follows. We introduce the dimensionless variables $\hat{r} = r/r_3$, $\hat{\theta} = \theta/\theta_{\max}$, where $\theta_{\max} = \vartheta_s(r_3) \ll 1$. Then

$$\begin{aligned}\Delta &= \frac{1}{r_3^2}\frac{\partial^2}{\partial\hat{r}^2} + \frac{1}{r_3^2\hat{r}}\frac{\partial}{\partial\hat{r}} + \frac{1}{r_3^2\theta\max\hat{r}^2}\frac{\partial^2}{\partial\hat{\theta}^2} \\ &= \frac{1}{r_3^2\theta_{\max}}(\frac{1}{\hat{r}^2}\frac{\partial^2}{\partial\hat{\theta}^2} + \theta_{\max}^2\frac{\partial^2}{\partial\hat{r}^2} + \frac{\theta_{\max}^2}{\hat{r}}\frac{\partial}{\partial\hat{r}}) \\ &= \frac{1}{r_3^2\theta_{\max}}(\frac{1}{\hat{r}^2}\frac{\partial^2}{\partial\hat{\theta}^2} + O(\theta_{\max}^2)).\end{aligned} \tag{5.6}$$

The solution of the simplified potential problem (5.2) with (5.5) can easily be found and is given by

$$\begin{aligned}V_s(r,\theta) = &\frac{qN_d}{2\varepsilon}r^2(\vartheta_s(r)\theta - \theta^2) + V(r,\vartheta_s(r))\frac{\theta}{\vartheta_s(r)} + \\ &+(V_g + \frac{qN_d}{C_{\text{ox}}}r\vartheta_s(r))(1-\frac{\theta}{\vartheta_s(r)}).\end{aligned} \tag{5.7}$$

Notice that here $\sin\vartheta_s(r)$ is replaced by $\vartheta_s(r)$, according to the thin-layer-approximation. The derivation of the problem formulation and the solution for the potential problem in the pn-junction will be completely analogous. Because this isn't of importance for the calculation of the current through the transition region (in the depletion region there is no current) we won't give the solution here.

5.2 Problem definition transition region

The derivation of the problem for the voltage $V = V(r,\theta)$ in the transition region G_t will be analogue to the one derived in subsection 4.1 for the drift region. Once again we obtain

$$\Delta V = 0, \tag{5.8}$$

where Δ is given by (5.4). The potential at radius r_1 and r_3 is set to V_1 and V_3, respectively. This yields

$$V(r_1,\theta) = V_1(\theta), \qquad V(r_3,\theta) = V_3(\theta). \tag{5.9}$$

In the depletion layers only a negligible amount of current can flow, so no current will enter the depletion regions. This yields

$$\mathbf{E}\cdot\mathbf{n}|_{\theta=\vartheta_s(r)} = 0, \qquad \mathbf{E}\cdot\mathbf{n}|_{\theta=\frac{\pi}{2}-\vartheta_1(r)} = 0. \tag{5.10}$$

To determine the normal $\mathbf{n}$ of the depletion layers we consider figure 8. Here we have sketched the boundary of the depletion layer at the oxide-silicon interface, with its normal and its position vector under an angle ϑ_s.

 ©Philips Electronics N.V. 2000

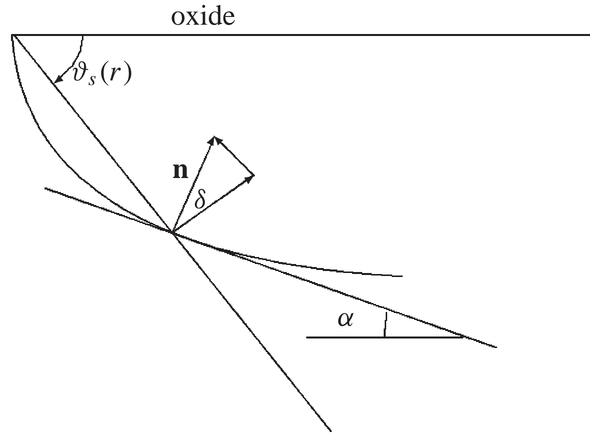

Figure 8: *Depletion layer at the oxide-silicon interface.*

From simple geometry it follows that

$$\delta = \vartheta_s - \alpha. \tag{5.11}$$

We can parameterise the curve by

$$x = r\cos\vartheta_s(r), \qquad y = r\sin\vartheta_s(r). \tag{5.12}$$

From this it follows that

$$\tan\alpha = \frac{dy}{dr}/\frac{dx}{dr} = \frac{\sin\vartheta_s + r\vartheta_s'\cos\vartheta_s}{\cos\vartheta_s - r\vartheta_s'\sin\vartheta_s}. \tag{5.13}$$

If we assume, as in the previous subsection, that ϑ_s is small, we get in first order approximation

$$\alpha \doteq \vartheta_s(r) + r\vartheta_s'(r). \tag{5.14}$$

This leads to

$$\mathbf{n} = \frac{1}{\sqrt{1+(r\vartheta_s')^2}}(-\mathbf{e}_\theta + r\vartheta_s'\mathbf{e}_r). \tag{5.15}$$

Substitution of (5.15) in (5.10) transforms the boundary condition into

$$r\vartheta_s'(r)\frac{\partial V}{\partial r}(r,\vartheta_s(r)) - \frac{1}{r}\frac{\partial V}{\partial\theta}(r,\vartheta_s(r)) = 0, \tag{5.16}$$

and analogue

$$r\vartheta_1'(r)\frac{\partial V}{\partial r}(r,\frac{\pi}{2}-\vartheta_1(r)) + \frac{1}{r}\frac{\partial V}{\partial\theta}(r,\frac{\pi}{2}-\vartheta_1(r)) = 0. \tag{5.17}$$

6 Potential in transition region

In this section we will use the same methods as in section 4, in order to determine the potential $V(r,\theta)$ in the transition region. Firstly, we will derive an analytic solution for the potential and the current. Secondly, we will use a numerical method to calculate the solution.

©Philips Electronics N.V. 2000

6.1 First analytic approach

The first idea is that $\vartheta_s(r)$ and $\vartheta_1(r)$ vary slowly in r. In first order approximation we thus assume that they are both constant, say θ_s and θ_1 respectively. The problem for the potential $V(r,\theta)$ then simplifies to

$$\begin{aligned}
&\Delta V = 0, && \\
&\tfrac{\partial V}{\partial \theta}(r,\theta_s) = 0, && r_1 \le r \le r_3, \\
&\tfrac{\partial V}{\partial \theta}(r,\tfrac{\pi}{2}-\theta_1) = 0, && r_1 \le r \le r_3, \\
&V(r_1,\theta) = V_1(\theta), && \theta_s \le \theta \le \tfrac{\pi}{2}-\theta_1, \\
&V(r_3,\theta) = V_3(\theta), && \theta_s \le \theta \le \tfrac{\pi}{2}-\theta_1.
\end{aligned} \tag{6.1}$$

We will construct a collection of functions which satisfy the differential equation $(6.1)^1$ and the homogeneous linear conditions $(6.1)^{2+3}$. To that end we use the method of separation, and search for functions of the form

$$V(r,\theta) = F(r)G(\theta). \tag{6.2}$$

Substitution of (6.2) in $(6.1)^1$ leads to

$$\frac{r^2F''(r) + rF(r)}{F(r)} = -\frac{G''(\theta)}{G(\theta)} = \lambda, \tag{6.3}$$

with λ constant. Together with the homogeneous conditions the problem transforms to

$$\begin{aligned}
&G''(\theta) + \lambda G(\theta) = 0, \qquad && r^2F''(r) + rF(r) - \lambda F(r) = 0 \\
&G'(\theta_s) = G'(\pi/2 - \theta_1) = 0. &&
\end{aligned} \tag{6.4}$$

Because (6.4) is a regular Sturm-Louville problem, theorem 2.4.6 of [5] gives us that there are an infinite amount of eigenvalues $\lambda_1 \le \lambda_2 \le ....$, and that the eigenfunctions form a complete system. From simple analysis we derive that the sought collection of functions is formed by

$$\{1, \log r, r^{n\pi/\xi}\cos\frac{n\pi}{\xi}(\theta-\theta_s), r^{-n\pi/\xi}\cos\frac{n\pi}{\xi}(\theta-\theta_s)\}, \qquad n = 1,2,... \tag{6.5}$$

Here ξ is defined as

$$\xi = \frac{\pi}{2} - \theta_s - \theta_1. \tag{6.6}$$

We assume that the solution can be written as

$$V(r,\theta) = a_0 + a_1\log r + \sum_{n=1}^{\infty}(a_n r^{\frac{n\pi}{\xi}} + b_n r^{-\frac{n\pi}{\xi}})\cos\frac{n\pi}{\xi}(\theta-\theta_s). \tag{6.7}$$

We can determine the coefficients from the inhomogenous conditions $(6.1)^{4+5}$, if we write V_1 and V_3 as

$$V_j(\theta) = c_{j_1} + \sum_{n=1}^{\infty} c_{j_n}\cos\frac{n\pi}{\xi}(\theta-\theta_s), \qquad j = 1,3. \tag{6.8}$$

 ©Philips Electronics N.V. 2000

The coefficients c_{j_n} are given by

$$c_{j_n} = \frac{2}{\xi} \int_{\theta_s}^{\pi/2-\theta_1} V_j(\theta) \cos \frac{n\pi}{\xi}(\theta - \theta_s) d\theta, \qquad j = 1, 3. \tag{6.9}$$

Notice that this solution is identical to the one suggested by Van de Ven e.o., [4] for the case $V_1 \equiv V_s$ and $V_3 \equiv V_d$. We have determined the solution for two different situations. For the numerical implementation, see Appendix B. Firstly, we consider constant and equal boundary conditions, i.e. $V_1(\theta) = V_3(\theta) \equiv V_d$. In that case we know the exact solution of (5.8)-(5.10), i.e. $V(r,\theta) \equiv V_d$. Our program gives the same solution, see figure 9. Here the solution is shown in the (r,θ)-field. For

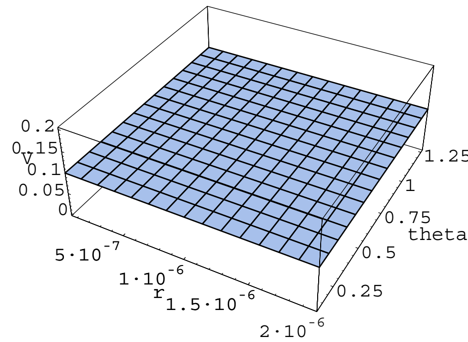

Figure 9: *Solution $V(r,\theta)$ with boundary conditions $V_1 = V_3 \equiv V_d = 0.1V$.*

other boundary conditions we don't know the exact solution of (5.8)-(5.10). In that case we have to estimate how accurate the analytic solution (6.7) is. In the derivation of the analytic solution we have assumed that ϑ_s and ϑ_1 are almost constant. We have to check whether the solution (6.7) satisfies this condition. We have seen before that

$$\vartheta_s(r) = \frac{k_s}{qN_d r}\left(\sqrt{V(r,\vartheta_s(r)) - V_g + V_{\text{Si}}} - \sqrt{V_{\text{Si}}}\right). \tag{6.10}$$

We determine $\vartheta_s(r)$ with the analytic solution and plot the thickness of the depletion layer, i.e. $r\vartheta_s$. The result can be seen in figure 10. We see that for constant boundary conditions the thickness of

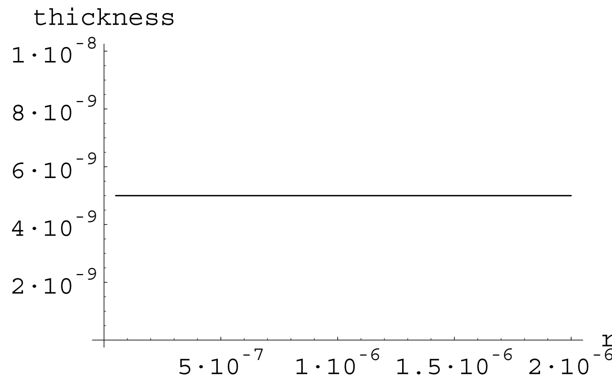

Figure 10: *Thickness of depletion region at gate-silicon interface.*

©Philips Electronics N.V. 2000

the depletion region is constant, so ϑ_s will behave as $1/r$. In that case we do not satisfy the previous assumption of nearly constant ϑ_s. This makes it impossible to tell how accurate the analytic solution (6.7) will be.
We will try to make an adjustement to the boundary conditions to achieve nearly constant ϑ_s and ϑ_1. We expect that at radius r_1 the potential V wil be a function of θ, because $V_1(\theta_s) \doteq V_g$, $V_1(\frac{\pi}{2} - \theta_1) \doteq V_b$ and $V_1(\frac{\pi}{4}) \doteq V_s$. Therefore we construct a polynomial of degree two for which these conditions yield and define V_1 as this polynomial. We set V_3 to the constant potential V_d. The analytic solution (6.7) is shown in figure 11. We have plotted the thickness of the depletion region for this situation

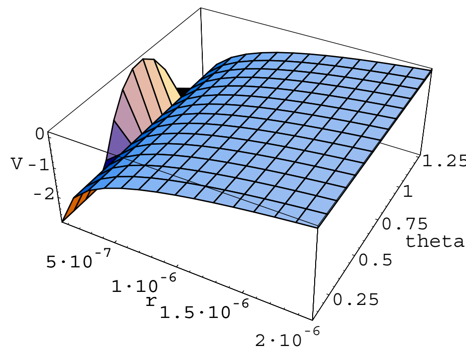

Figure 11: *Solution $V(r,\theta)$ with boundary conditions $V_1 = Pol_2(\theta)$ and $V_3 = V_d = 0.1V$.*

in figure 12. We observe that these boundary conditions also don't result in depletion layers with

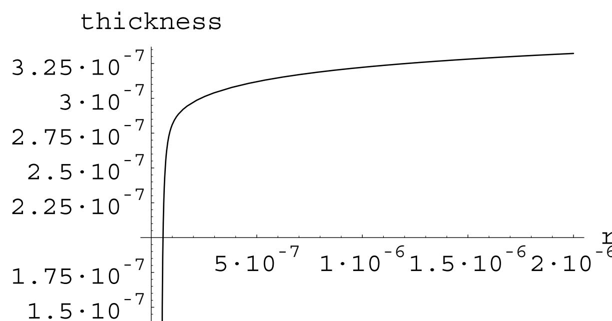

Figure 12: *Thickness of depletion region at gate-silicon interface.*

constant angle ϑ_s, which is in contrast to the assumption made at the beginning of this subsection. It seems that ϑ_s and ϑ_1 are not constant. However, from these calculations it seems reasonable to assume that the thickness of the depletion regions is constant, except for r small. In the next section we will find an analytic solution in which we apply the above assumption.

 ©Philips Electronics N.V. 2000

6.2 Analytic solution

In this subsection we will use the same technique as in subsection 4.1. We assume that $\delta = (V_d - V_s)/V_{\rm Si}$ is small and that the solution V can be expanded in a series, analogue to (4.8), as

$$\begin{aligned} &V(r,\theta) = V_0(r,\theta) + V_1(r,\theta)\delta + ..., \\ &\vartheta_s(r) = \theta_s(r) + \theta_{s1}(r)\delta + ..., \\ &\vartheta_1(r) = \theta_1(r) + \theta_{11}(r)\delta + ... \end{aligned} \tag{6.11}$$

The problem formulation for V_0 then reads

$$\begin{aligned} &\Delta V_0 = 0, \\ &V_0(r_1,\theta) = V_s, \\ &V_0(r_3,\theta) = V_s, \\ &r\theta_s'(r)\tfrac{\partial V_0}{\partial r}(r,\theta_s(r)) - \tfrac{1}{r}\tfrac{\partial V_0}{\partial \theta}(r,\theta_s(r)) = 0, \\ &r\theta_1'(r)\tfrac{\partial V_0}{\partial r}(r,\tfrac{\pi}{2}-\theta_1(r)) + \tfrac{1}{r}\tfrac{\partial V_0}{\partial \theta}(r,\tfrac{\pi}{2}-\theta_1(r)) = 0. \end{aligned} \tag{6.12}$$

The solution of problem (6.12) is $V_0(r,\theta) \equiv V_s$. If we define α and β according to

$$\alpha = \frac{k_s}{qN_d}(\sqrt{V_s - V_g + V_{\rm Si}} - \sqrt{V_{\rm Si}}), \qquad \beta = \frac{k_b}{qN_d}\sqrt{V_s - V_b}, \tag{6.13}$$

we derive the following problem formulation for V_1

$$\begin{aligned} &\Delta V_1 = 0, \\ &V_1(r_1,\theta) = 0, \\ &V_1(r_3,\theta) = V_{\rm Si}, \\ &\alpha\tfrac{\partial V_1}{\partial r}(r,\tfrac{\alpha}{r}) + \tfrac{\partial V_1}{\partial \theta}(r,\tfrac{\alpha}{r}) = 0, \\ &\beta\tfrac{\partial V_1}{\partial r}(r,\tfrac{\pi}{2}-\tfrac{\beta}{r}) - \tfrac{\partial V_1}{\partial \theta}(r,\tfrac{\pi}{2}-\tfrac{\beta}{r}) = 0. \end{aligned} \tag{6.14}$$

The area where (6.14) is defined is sketched in figure 13. To solve (6.14) we introduce new variables ρ and ϕ; see figure 13. The problem formulation for V_1 in the new variables reads, in first order approximation,

$$\begin{aligned} &\Delta V_1(\rho,\phi) = 0, \\ &V_1(\gamma,\phi) = 0, \\ &V_1(r_3 - r_1,\phi) = V_{\rm Si}, \\ &\tfrac{\partial V_1}{\partial \phi}(\rho,0) = 0, \\ &\tfrac{\partial V_1}{\partial \phi}(\rho,\pi/2) = 0, \end{aligned} \tag{6.15}$$

where γ is defined by

$$\gamma = r_1 - \sqrt{\alpha^2 + \beta^2}, \tag{6.16}$$

so γ is small. Problem (6.15) can be solved with separation of variables according to subsection 6.1. Elaboration yields

$$V_1(\rho,\phi) = \frac{\log\frac{\rho}{\gamma}}{\log\frac{r_3-r_1}{\gamma}}V_{\rm Si}. \tag{6.17}$$

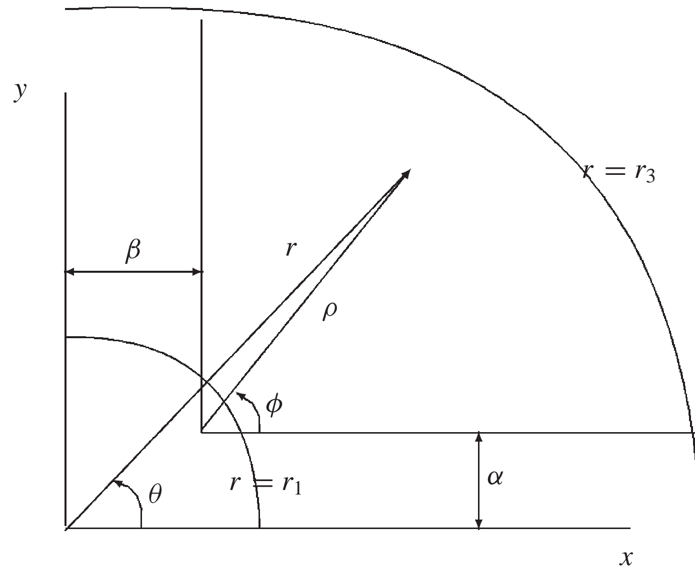

Figure 13: *Transition region in new variables ρ and ϕ.*

To transform the solution (6.17) back to the old coordinates (r, θ), we use the relations

$$r \cos\theta = \rho \cos\phi + \beta, \qquad r \sin\theta = \rho \sin\phi + \alpha. \tag{6.18}$$

Reformulation of (6.18) gives

$$\phi = \arctan \frac{r \sin\theta - \alpha}{r \cos\theta - \beta}, \qquad \rho = \frac{r \sin\theta - \alpha}{\sin\phi}. \tag{6.19}$$

We have plotted the solution (6.17) in figure 14. The solution is not plotted in the total region because the transition region is bounded by the depletion layers. We see that the solution is almost independent

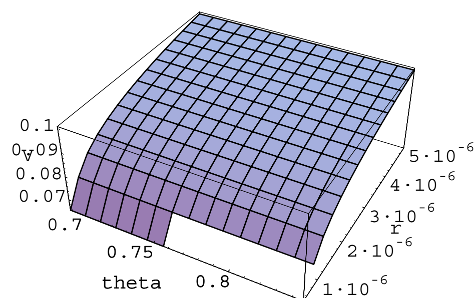

Figure 14: *Analytic solution $V(r, \theta)$, according to (6.17); $V_1 = 0V$ and $V_3 = 0.1V$.*

of θ, which implies that the current will mainly flow in the $\mathbf{e}_r$-direction.

 ©Philips Electronics N.V. 2000

6.3 First numerical approach

In the process of deriving the analytic solution we have made some assumptions about the shape of the transition region and the applied voltages, which can't always be satisfied. To obtain a method that can be applied without these asumptions, we will use numerical techniques. In this subsection we will use the same method as in subsection 4.2. We assume that the current through the drift region is known. Furthermore we assume that the current is only directed in the $\mathbf{e}_r$-direction. The potential then only depends on the radius r. As a result, the current density reads

$$J_r = q\mu_n n(r,\theta)\frac{dV(r)}{dr}. \tag{6.20}$$

Analogous to (4.16) we derive that the total current I through the channel is given by

$$I = W\mu_n \frac{dV(\xi)}{d\xi}(qN_d\frac{\pi}{2}\xi - Q_3(V(\xi)) - Q_1(V(\xi))). \tag{6.21}$$

Integration of (6.21) with respect to ξ from r_1 to r yields

$$\begin{aligned} \tfrac{(r-r_1)I}{W\mu} = \;& qN_d\tfrac{\pi}{2}(rV(r) - r_1V_s - \textstyle\int_{r_1}^{r} V(\xi)d\xi) - k_s[\tfrac{2}{3}\{(V(r) - V_g + V_{\text{Si}})^{3/2} + \\ & -(V_s - V_g + V_{\text{Si}})^{3/2}\} - \sqrt{V_{\text{Si}}}(V(r) - V_s)] + \\ & -\tfrac{2}{3}k_b[(V(r) - V_b)^{3/2} - (V_s - V_b)^{3/2}]. \end{aligned} \tag{6.22}$$

From this expression we determine $V(r)$ numerically for every r. The integral in the right-hand-side is determined numerically with the previously calculated values. For the program, see appendix C. The potential as a function of r can be seen in figure 15. To determine the correct value for the current

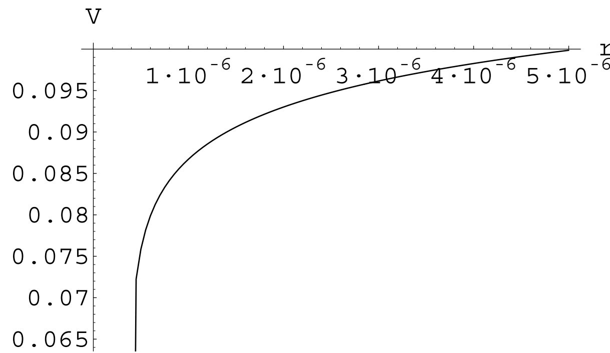

Figure 15: *Numerically determined potential $V(r)$ in transition region, $V_d = 1V$.*

I we try several values to match the condition $V(r_3) = V_d$. Notice that $V(r_1) = V_s$ is automatically satisfied. The shape of the potential $V(r)$ obviously coincides with the analytic solution found in the previous subsection, see figure 14.

6.4 Numerical solution

In the previous section we have presented a numerical method to determine the potential in the transition region. This method was based on determination of the roots of (6.22), which is an instabel

process when performed with Mathematica. Because we want solutions that are easy to determine and reliable in all cases, we will derive in this subsection another numerical method. We are not really interested in the potential in the transition region, but we want to determine the current I as a function of the applied voltages, in particular V_d. For the derivation of this method we will discretisize equation (6.21) using Euler Forward. This yields

$$V(r + \triangle r) = V(r) + \triangle r \frac{I}{W\mu_n} \frac{1}{qN_d \frac{\pi}{2} r - Q_3(V(r)) - Q_1(V(r))}, \tag{6.23}$$

where Q_3 and Q_1 are given by

$$\begin{aligned} Q_1(V(r)) &= k_b \sqrt{V(r) - V_b}, \\ Q_3(V(r)) &= \begin{cases} k_s(\sqrt{V(r) - V_g + V_{\text{Si}}} - \sqrt{V_{\text{Si}}}), & V(r) > V_g, \\ -C_{\text{ox}}(V_g - V(r)), & V(r) \leq V_g. \end{cases} \end{aligned} \tag{6.24}$$

With formula (6.23) we determine the potential in the transition region for given current I. We start with $V(r_1) = V_s$, and subsequently determine the potential V at a radius $\triangle r$ further than the previously calculated potential, according to (6.23), until we reach the boundary $r = r_3$ or until the two depletion regions touch each other. The voltage V at radius r_3 is V_d. So, instead of applying the voltage V_d and then determine the current I, we apply the current I and determine the matching voltage V_d. In case the depletion layers touch each other, the transition region becomes infinitely small at a certain radius and gets pinched-off. The opening through which the current must flow becomes infinitely small and the current thus reaches its maximum. The voltage V_d at which this occurs is called the pinch-off voltage. If the voltage V_d is made larger than the pinch-off voltage the current remains constant. We have implemented the method described above in Mathematica; see Appendix D. In figure 16 we

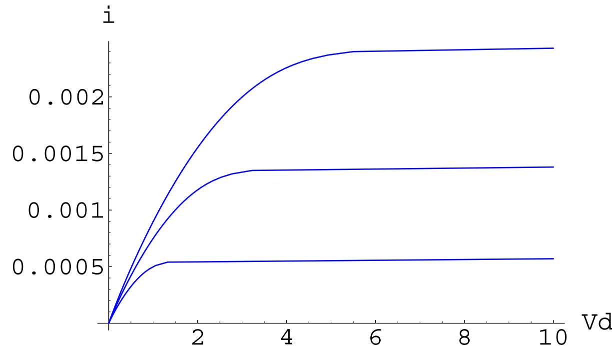

Figure 16: *Numerically determined characteristics in transition region, for f.l.t.r.* $V_g = 2, 1$ *and* 0V.

observe the characteristics obtained by this method for three different values of the gate-voltage , i.e. $V_g = 0$, 1 and 2V. We observe that for small values of V_g the current is pinched off at small values of V_d and that the current reaches its maximum there. From the calculated data we next determine the shape of the transition region for a given current I or, equivalently, a given voltage V_d. We have done that for two different bias situations. In the first situation we have chosen $V_b = 0$V, $V_g = 0$V, $V_s = 0$V and $I = 5 \cdot 10^{-4}$A. In that case no accumulation occurs; see figure 17. The oxide-silicon interface is drawn at the bottom of the picture, so the picture should actually be considered upside down. In the second situation we have chosen the values $V_b = 0$V, $V_g = 3$V, $V_s = 0$V and $I = 5 \cdot 10^{-3}$A. In that

 ©Philips Electronics N.V. 2000

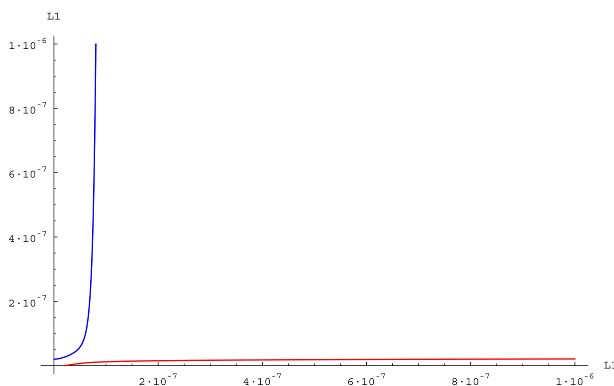

Figure 17: *Transition region and depletion layers,* $V_g = 0V$*.*

case there will be an area at the oxide-silicon interface where accumulation occurs as well as an area where depletion occurs. Remember that in case of accumulation the thickness of the depletion layer at the oxide-silicon layer is zero; see figure 18: for $r_1 = 10^{-8}\text{m} \leq r \leq 2 \cdot 10^{-7}\text{m}$ an accumulation

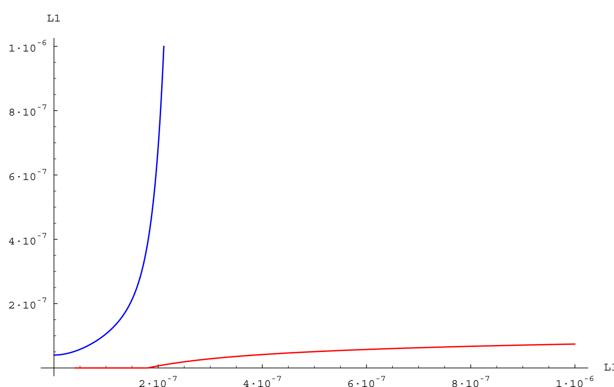

Figure 18: *Transition region and depletion layers,* $V_g = 3V$*.*

sheet is formed, whereas for $r \geq 2 \cdot 10^{-7}$m a depletion layer is formed. Also notice that the depletion layer at the *pn*-junction is considerably thicker than at the oxide-silicon interface.

7 Comparison

We have derived several methods to solve the potential and the current in the transition region as a function of the applied voltages. The most accurate solution is of course the last numerical method, described in subsection 6.4. In large circuits, with its many thousands of transistors, a numerical method is not an option. That's why we want to test how well the analytic solutions fit the data obtained from the numerical method.

©Philips Electronics N.V. 2000

7.1 Drift and transition region

We have seen in the previous sections that the geometry and the derived solutions for the drift and transition region differ a lot. Within Philips for both regions the same model, i.e. MOS Model 31 (MM31), is used. In practice, measurements are done to obtain the characteristics as derived in the previous section. The parameters of MOS Model 31 are then used to fit the model on the measured curves. We want to know whether it is justified to use MM31 for the transition region. To investigate this we will try to fit MM31 on the numerically calculated characteristics for the transition region. We have a couple of parameters we can use to fit MM31 on the data, see [1] and [3]. They are the resistance R_{on}, the pinch-off voltage V_p and the parameter p_{sat}. We will use these parameters to fit the situation of zero applied voltages, i.e. V_s, V_b and V_g are zero. We will fit R_{on} such that the behaviour of the characteristic for V_d small is the same, V_p and p_{sat} such that the behaviour for V_d large is the same. For the program see Appendix E. The fit gives $R_{\text{on}} = 1150\Omega$, $V_p = 0.7\text{V}$ and $p_{\text{sat}} = 3$. The result of this fit can be seen in figure 19. The idea is that these values will also give accurate results

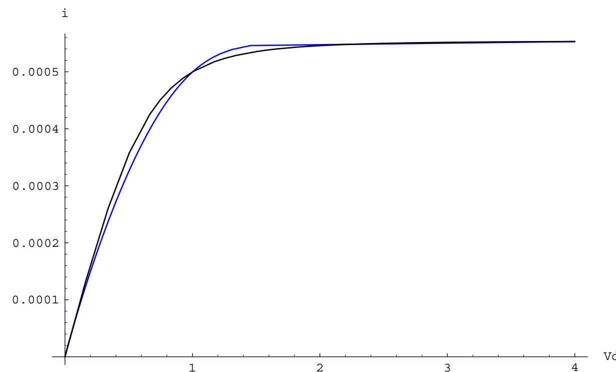

Figure 19: *MOS Model 31 fits on numerically determined characteristic, calculated according to (6.23)-(6.24), by taking* $R_{\text{on}} = 1150\Omega$, $V_p = 0.73V$ *and* $p_{\text{sat}} = 3$.

for other values of the applied voltages. Only if this is true, it is justified to use MM31 to characterize the transition region. To check this we choose a different value for the gate-voltage, i.e. $V_g = -2\text{V}$. The result can be seen in figure 20, where MOS Model 31 predicts too much current. Thus, the fit is

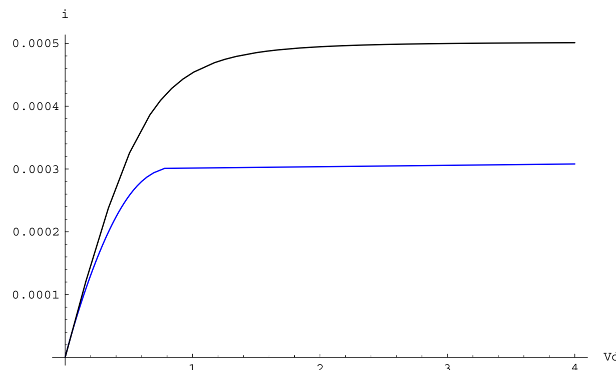

Figure 20: *MOS Model 31 and numerically determined characteristic, calculated according to (6.23)-(6.24), for* $V_g = -2V$.

©Philips Electronics N.V. 2000

insufficient.
Within Philip Research a special program, called Iccap is used to fit simulated curves on the measurements. It uses several least-square techniques to optimize the parameters of a given model to fit the data. We have used this program to obtain better fits. We have numerically determined the characteristics of Ids versus Vds for V_g is 0, 5 and 10V. The parameters we use to optimize the fit are R_{on}, R_{sat}, V_{sat}, p_{sat} and V_p. For the definition of these parameters, see Modelbook [3]. The result of the fit can be seen in figure 21. Here we have also optimized the first derivative $\frac{\partial I_{ds}}{\partial V_{ds}}$. This is essential

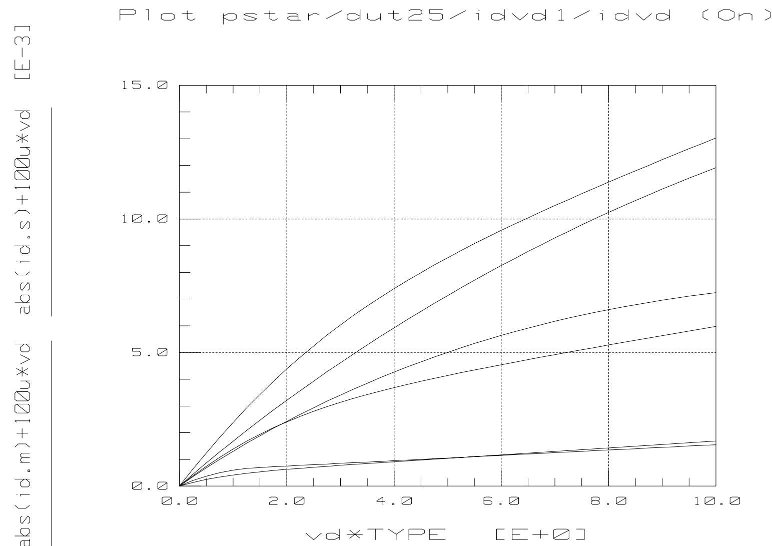

Figure 21: I_{ds} *versus* V_{ds} *for* $V_g = 0$*, 5 and 10V, and* $V_b = 0V$ *according to MM31 and (6.23)-(6.24).*

because the curves should have the same behaviour for the same values of V_d. We don't want, for instance, that for a certain value of V_d the measured current is pinched-off whereas MM31 shows an ohmic current. The optimal parameters determined by use of Iccap are $R_{\text{on}} = 2063\Omega$, $R_{\text{sat}} = 2116\Omega$, $V_{\text{sat}} = 15.5$V, $p_{\text{sat}} = 1.97$ and $V_p = 2.15$V

7.2 Analytic and numerical method

In this subsection we test how good the analytic solution (6.17) matches the characteristics determined by (6.23)-(6.24). Therefore we integrate the potential (6.17), found in subsection 5.2, and substitute this expression in equation (6.22), in which we replace r by r_3. That way we get an easy to evaluate expression for the current as a function of the voltage V_d. We still have one parameter to fit the data, that is the pinch-off voltage at zero gate and substrate voltage. We obtain for V_p the same value as in the previous section, i.e. 0.7V. The characteristics obtained are identical to figure 19, so we won't plot them here. To check whether the analytic solution fits the data better than MM31 for other values of the gate -and substrate voltage, we set V_g to -2V and plot the result in figure 22. We can see that the analytic solution (6.17) is a better approximation of the numerically determined data than MOS Model 31.

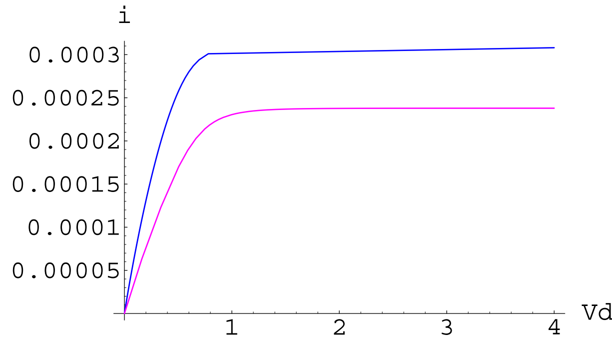

Figure 22: *Analytic (6.17) and numerical (6.23) characteristic for* $V_g = -2V$.

8 Discussion

In the previous section we have seen that the different methods give different characteristics. Here, we will try to explain this difference. To get some insight in the differences we plot the potential for $V_g = 4$V. The result is shown in figure 23. The numerical solution (6.23) starts at the correct

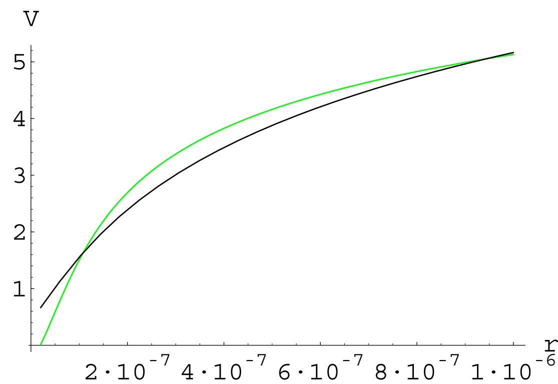

Figure 23: *Potential* $V(r)$ *(analytic and numerical) for* $V_g = 4V$ *and* $V_d = 5V$.

value $V = 10^{-6}$V. The analytic solution (6.17) does not fit this boundary condition. This is caused by the fact that the depletion layers change rapidly for r in the neighbourhood of r_1, as we have seen in subsection 6.1. This is inconsistent with the assumption of the analytic solution that the depletion layers are almost constant. However, for the largest part of the transition region the depletion layers are in first order approximation constant, so that the analytic solution is valid there. Because the plotted potentials differ, the corresponding electric fields also differ. We have plotted the electric field; see figure 24. We observe that the numerically calculated field is larger than the analytic field at $r = r_1$. The curves differ considerately for small values of r, which is the main cause of the difference in the obtained characteristics.
If we take a closer look at figure 24, we notice that the electric field is very large. It appears that the field exceeds the value of $7 \cdot 10^3 \mathrm{Vm}^{-1}$, which is the field at which velocity saturation occurs, in almost the whole area. Thus, the saturation field is the electric field at which the electrons won't move at a higher speed with increasing electric field. Figure 24 shows that almost everywhere in the transition

 ©Philips Electronics N.V. 2000

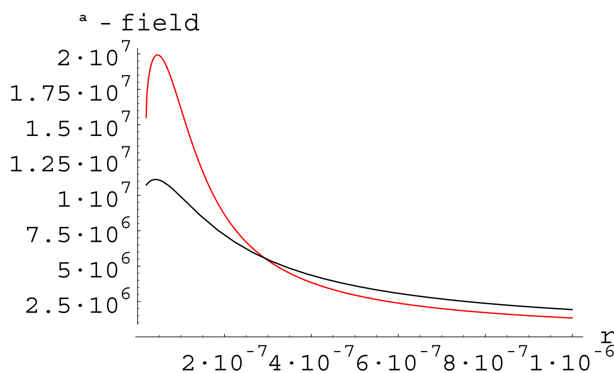

Figure 24: *Electric field (analytic and numerical) for* $V_g = 4V$ *and* $V_d = 5V$.

region saturation will occur at these values of V_d and V_g.

9 Conclusions and recommendations

In the previous sections we have derived models for the drift and transition region. We have seen that these regions differ a lot in geometry. It has also been made clear that the geometry of the transition region makes it much more difficult to derive an analytic solution than in the case of the drift region. This difference is due to the wedge shape of the area and the block shape of the boundaries. With help of a numerical method we have been able to derive the characteristics I_{ds} versus V_{ds} for the transition region. Within Philips MOS Model 31 is used to describe the behaviour of the transition region. We have used Iccap, a program that is also used at Philips to fit measured data on the curves of MM31, to see how well MM31 fits the numerically determined data. It is clear that the fit is not by far perfect. The question, however, is whether the fits are insufficient to use MM31 for the transition region. This is not a question that easily can be answered. The curves differ a lot and it is very hard for MM31 to obtain the same behaviour as the data. From this we could conclude that the fit is insufficient. However, in practice a device consists of three regions, i.e. a channel, the transition region and the drift region. The characteristic curves that are measured are the sum of the characteristics of the seperate parts. If we consider the device as whole we have a lot more parameters to fit the data. Errors that are made in the transition region could then be corrected in for instance the drift region. However, still a concern raises about the stability of the MOS Model 31 parameters that are used to describe the transition region. Small values of, for instance, the pinch-off voltage are likely to cause convergence problems in MM31.
Although a lot can thus be solved by coupling different regions and using the extra parameters you get in that way, it is clear that the drift and transition region differ not only in geometry but also in electrical behaviour. Because of the wedge shape of the transition region, the opening between the depletion layers is very small. This implies that the current can easily be pinched off. This in contrast to the drift region where there is a relative large opening between the depletion layers. Another effect of the small opening is a high electric field. The current has to flow through a small opening so the electric field has to be very high there. It is plausible that in (the largest part) of the transition region a saturation current will flow. This has to be verified by experiment, if possible, and Medici (finite-element method) simulations. If saturation occurs in nearly the whole transition region, MM31

should be used with V_{sat} sufficiently low. Also a further analytic investigation of the transition region is advisable. The derived solution (6.17) could be expanded to higher order terms. Special attantion should then be paid to the first part of the transition region, where a different solution has to be sought. Here the depletion layers differ a lot in size as a function of the radius r, so different methods and techniques have to be used to derive an analytic solution.

 ©Philips Electronics N.V. 2000

A Numerical determination potential in drift region

```
Vb = 0;
Vg = -10;
Vs = 0;
Vd = 1;
Xs = 10 10^-9;
Xd = 1 10^(-6);;
q = 1.602 10^(-19);
Nd = 10^(22);
Na = 10^(22);
epsox = 0.3453 10^(-11);
Tox = 200 10^(-9);
eps = 1.036 10^(-11);
Ks = Sqrt[2 q Nd eps];
Kb = Sqrt[2 q eps Na Nd/(Na + Nd)];
Cox = epsox/Tox;
Vsi = q eps Nd/(2 Cox^2);
mu = 1370 10^(-4);
W = 10 10^(-6);
Te = 2 10^(-6);
Ron = (Xd - Xs)/(W mu q Nd Te);
c = W mu (Vd - Vs)/(Xd - Xs);
Iohm = (Vd - Vs)/Ron - c Ks (2/3/(Vd - Vs) ((Vd
    - Vg + Vsi)^(3/2) - (Vs - Vg + Vsi)^(3/2)) -
    Sqrt[Vsi])- c Kb 2/3/(Vd - Vs) ((Vd - Vb)^(3/2)
    - (Vs - Vb)^(3/2)) ;
rhs1 = q Nd Te  Vs - 2/3 Ks (Vs - Vg + Vsi)^(3/2) +
   Ks Sqrt[Vsi] Vs - 2/3 Kb (Vs - Vb)^(3/2);
rhs2[b_] = (b - Xs) Iohm/(W mu);
lhs[a_] =  q Nd Te (a) - 2/3 Ks (a - Vg + Vsi)^(3/2)
 - 2/3 Kb (a - Vb)^(3/2) +   Ks Sqrt[Vsi] a;

Clear[V];
aantal = 100;
For[x = Xs, Xs <= x <= Xd, x = x + (Xd - Xs)/aantal,
  V[x] = a /.
      Last[FindRoot[
          lhs[a] == rhs1 + rhs2[x], {a,
            If[x > Xd, V[x - (Xd - Xs)/aantal], 0]}]]]
MOS31Lijst = Table[{x, V[x]}, {x, Xs, Xd, (Xd - Xs)/aantal}];
ListPlot[MOS31Lijst]
```

©Philips Electronics N.V. 2000

B Exact solution transition region

```
Vb = -7;
Vg = -10;
Vs = 0;
Vd = 0.1;
th1 = 0.3;
ths = 0.1;
r1 = 0.5 10^(-7);
r3 = 2 10^(-6);
q = 1.602 10^(-19);
Nd = 10^(22);
Na = 0.5 10^(22);
epsox = 0.3453 10^(-11);
Tox = 10 10^(-9);
eps = 1.036 10^(-11);
Ks = Sqrt[2 q Nd eps];
Cox = epsox/Tox;
Vsi = q eps Nd/(2 Cox^2);
Vb1 = (r1 th1)^2 q Nd (Na+Nd)/(2 eps Na) + Vb;
Vg1 = (ths q Nd r1/Ks+Sqrt[Vsi])^2 + Vg - Vsi;
a0 = (Vb1 - Vg1 - (Pi/2-th1-ths)/(Pi/4-ths) (Vs
  -Vg1))/((Pi/2-   th1)^2 - ths^2 - (Pi/2-
 th1-ths) (Pi/4+ths));
b0 = (Vs-Vg1-Pi^2/16 a0+ths^2 a0)/(Pi/4-ths);
c0 = Vg1 - a0 ths^2 - b0 ths;
x = Pi/2 - th1 - ths;
a1 = a0;
b1 = 2 a0 ths + b0;
c1 = a0 ths^2 + b0 ths + c0;
c[0] = 1/3 a1 x^2 + 1/2 b1 x + c1;
c[n_] = (-1)^n 4 a1 x^2/(n Pi)^2 + 2 b1 x/(n Pi)^2 ((-1)^n - 1);
a[0] = c[0];
a[n_] = (r3^(-n Pi/x)-r1^(-n Pi/x))/((r1/r3)^(n Pi/x)-(r3/r1)^(n Pi/x)) c[n];
b[n_] = (r1^(n Pi/x)-r3^(n Pi/x))/((r1/r3)^(n Pi/x)-(r3/r1)^(n Pi/x)) c[n];
a2[1] = (Vd - c[0])/Log[r3/r1];
a2[0] = c[0] - a2[1] Log[r1];
b2[n_] = c[n]/(r1^(-n Pi/x) - r1^(n Pi/x) r3^(-2 n Pi/x));
a2[n_] = -b2[n] r3^(-2 n Pi/x);
V[r_, th_] =
    a[0] + Sum[(a[n] r^(n Pi/x)+b[n] r^(-n Pi/x)) Cos[
            n Pi (th - ths)/x], {n, 1, 100}];
V1[r_, th_] = a2[0] + a2[1] Log[r] +
      Sum[(a2[n] r^(n Pi/x) +
      b2[n] r^(-n Pi/x)) Cos[n Pi (th - ths)/x], {n, 1, 300}];
```

 ©Philips Electronics N.V. 2000

C Numerical determination potential transition region.

```
Vb = -7;
Vg = -10;
Vs = 0;
Vd = 0.1;
th1 = 0.3;
ths = 0.1;
r1 = 0;
r3 = 5 10^(-6);;
q = 1.602 10^(-19);
Nd = 10^(22);
Na = 0.5 10^(22);
epsox = 0.3453 10^(-11);
Tox = 10 10^(-9);
eps = 1.036 10^(-11);
Ks = Sqrt[2 q Nd eps];
Kb = Sqrt[2 q eps Na Nd/(Na + Nd)];
Cox = epsox/Tox;
Vsi = q eps Nd/(2 Cox^2);
mu = 1370 10^(-4);
W = 1 10^(-6);
Te = 2 10^(-6);
aantal = 100;
Iohm = 6.88 10^-7;
rhs1 = -2/3 Ks (Vs - Vg + Vsi)^(3/2) - Ks Sqrt[Vsi] Vs -
      2/3 Kb (Vs - Vb)^(3/2);
rhs2[b_] = (b - r1) Iohm/(W mu);
lhs[b_] = q Nd Pi/2 (a b -
   Sum[V[r1 + t (r3 - r1)/aantal] (r3 - r1)/aantal,
   {t,0, (b - r1) aantal/(r3 - r1) - 1}] -
   a (r3 - r1)/aantal) -   2/3 Ks (a - Vg + Vsi)^(3/2)
   - 2/3 Kb (a - Vb)^(3/2) -   Ks Sqrt[Vsi] a;

Clear[V];
For[r = r1, r1 <= r <= r3, r = r + (r3 - r1)/aantal,
  V[r] = a /. Last[FindRoot[lhs[r] == rhs1 + rhs2[r], {a, 0}]]]
MOS31Lijst = Table[{r, V[r]}, {r, r1, r3, (r3 - r1)/aantal}];
tek1 = ListPlot[MOS31Lijst, PlotJoined -> True]
```

©Philips Electronics N.V. 2000

D Numerical method for characteristics

```
Vb = 0;
Vg = 0;
Vs = 10^-6;
r1 = 40 10^-9;
r3 = 1 10^(-6);;
q = 1.602 10^(-19);
Nd = 10^(22);
Na = 10^(22);
epsox = 0.3453 10^(-11);
Tox = 100 10^(-9);
eps = 1.036 10^(-11);
Ks = Sqrt[2 q Nd eps];
Kb = Sqrt[2 q eps Na Nd/(Na + Nd)];
Cox = epsox/Tox;
Vsi = q eps Nd/(2 Cox^2);
mu = 1370 10^(-4);
W = 10 10^(-6);

aant = 100;
pinch = 0;
eindwaardeV = 4;
eindwaardeI = 7 10^-4;
punten = Table[{
  For[r = r1; aantal = 1000; dr = (r3 - r1)/aantal;
  If[pinch == 0, Vt = Vs, Vt = eindwaardeV], r <= r3 && pinch == 0,
    r = r + dr,
    q3 = Kb Sqrt[Vt - Vb];
    q1 = If[Vt > Vg,
    Ks (Sqrt[Vt - Vg + Vsi] - Sqrt[Vsi]), -Cox (Vg - Vt)];
    l1 = If[Vt > Vg, Ks (Sqrt[Vt - Vg + Vsi] - Sqrt[Vsi])/(q Nd), 0];
    If[q Nd Pi/2 r - q3 - l1 q Nd > 0, pinch = 0, pinch = 1];
    Vt = If[pinch == 0, Vt + dr Id/(W mu (q Nd Pi/2 r - q3 - q1)),
         eindwaardeV - 0.00001];];
     Vt, Id},
    {Id, 0, eindwaardeI, eindwaardeI/aant}];

punten1 = Select[punten, First[#] < eindwaardeV &];
tek3 = ListPlot[punten1, PlotJoined -> True, AxesLabel -> {Vd, i},
    PlotRange -> All, PlotStyle -> RGBColor[0, 0, 1]]
```

 ©Philips Electronics N.V. 2000

E Fit of MM31

```
nr = 2;
Ron = 1/((Last[punten1[[nr]]]-Last[punten1[[1]]])/(
 First[punten1[[nr]]] - Vs) +
 Ks W mu/(Xd - Xs) ((First[punten1[[nr]]]-Vg+Vsi)^(1/2) -
 Sqrt[Vsi])+ Kb W mu/(Xd - Xs)(First[punten1[[nr]]]-Vb)^(1/2)) ;
Te = (Xd - Xs)/(W mu q Nd)/Ron;
Xs = r1;
Xd = r3;
Rsat = 1000;
Vsat = 100000000;
deltaV = 10^-8;
psat = 3;
Vp0 = 0.74;
Qi = Ks (Sqrt[Vp0 + Vsi] - Sqrt[Vsi]) + Kb Sqrt[Vp0];
Vbsw = Vg - (Qi/Kb)^2;
Qm = Qi + Ks Sqrt[Vsi];
Vgsw = Vb - (Qm/Ks)^2 + Vsi;
Bp = Kb Qm/(Ks^2 - Kb^2);
Cp = (Qm^2 + Ks^2 (Vg - Vsi - Vb))/(Ks^2 - Kb^2);
If[Vb <= Vbsw,
    Vp = Vg + Qi/Cox + Kb^2/(2 Cox^2) -
        Kb/Cox Sqrt[(Kb/(2 Cox))^2 + Vg - Vb + Qi/Cox],
    If[Vg <= Vgsw, Vp = Vg - Vsi + (Qm/Ks)^2,
      Vp = Vb + 2 Bp^2 + Cp - 2 Bp Sqrt[Bp^2 + Cp]]];
Vsp = 1/2 (Vs + Vp - Sqrt[(Vs - Vp)^2 + deltaV]);
Vc = Vsat + Vp - Vsp - Sqrt[Vsat^2 + (Vp - Vsp)^2];
Vdp = Vsp + (Vd - Vs) Vc/((Vd - Vs)^psat + Vc^psat)^(1/psat);
c = W mu (Vd - Vs)/(Xd - Xs);
P0 = 0;
Vfb = 0;
Qi = q Nd Te - Kb Sqrt[P0];
Kb1 = Kb/(Qi Ron);
Ks1 = Ks/(Qi Ron);
Ks4 = Cox/(Qi Ron);
If[Vg - Vfb <= Vsp, Vap = Vsp,
    If[Vsp <= Vg - Vfb <= Vdp, Vap = Vg - Vfb, Vap = Vdp]];
Vdbp = Vdp - Vb + P0;
Vgb = Vg - Vfb - Vb + P0;
Vabp = Vap - Vb + P0;
Vdgp = Vdp - Vg + Vfb + Vsi;
Vsbp = Vsp - Vb + P0;
Vagp = Vap - Vg + Vfb + Vsi;
If[(Vb - P0) < Vsp,
 Ibdp = Kb1(2/3 (Vdbp^{3/2}-Vsbp^{3/2})-Sqrt[P0] (Vdp-Vsp)),
```

```
 If[Vsp <= Vb - P0 < Vdp,
 Ibdp = Kb1 (2/3 Vdbp^{3/2}-Sqrt[P0] (Vdp-Vb+P0)), Ibdp=0]];
Isdp = If[Vg - Vfb < Vdp,
 Ks1 (2/3 (Vdgp^{3/2}-Vagp^{3/2})-Sqrt[Vsi] (Vdp-Vap)),0];
If[Vg - Vfb > Vsp,
 Isap = Ks4 ((Vg-Vfb) (Vap-Vsp)-1/2 (Vap^{2}-Vsp^{2})),Isap=0];
IohmP = (Vdp - Vsp)/Ron - Ibdp - Isdp + Isap;
IohmDS = IohmP (1 + Ron/Rsat (Vd - Vdp)/Vsat);
tek4 = Plot[IohmDS, {Vd, Vs, eindwaardeV}]
```

 ©Philips Electronics N.V. 2000

References

[1] AARTS, A.C.T., *Background to MOS Model 31 for the Drift Region of High-Voltage MOS Devices*, Philips Research, Report nr. 7097, (1999), Company Restricted.

[2] KLOOSTERMAN, W.J., *The modeling of high voltage MOS transistors*, Philips Research Report nr. 6798, RWR-582-WK-94212-WK, (1994), Company Restricted.

[3] *MOST Modelbook*, 6th Ed., Philips Electronics N.V., (1998), Company Confidential.

[4] VAN DE VEN, A.A.F. E.O., *On compact models for high-voltage MOS devices*, University of Eindhoven, (2000).

[5] HAUTUS, M., *Analyse 5*, Department of mathematics and computing science, University of Eindhoven, (1998).

©Philips Electronics N.V. 2000

©Philips Electronics N.V. 2000

Author(s) I.E.M. Severens

Title The drift region of high-voltage MOS devices

Distribution

Nat.Lab./PI	WB-5	
PRL	Redhill, UK	
PRB	Briarcliff Manor, USA	
LEP	Limeil–Brévannes, France	
PFL	Aachen, BRD	
CP&T	WAH	
Director:	M.G. Collet	WAG-14
Department Head:	R. Woltjer	WAG-14

Abstract

J. van der Pol	Philips Semiconductors	Nijmegen
M. Swanenberg	Philips Semiconductors	Nijmegen
J. Bruines	Philips Semiconductors	Nijmegen
J. Paasschens	Philips Semiconductors	Albuquerque
B. Redman-White	Philips Semiconductors	Southampton
L. Lengowski	ED&T Analogue Simulation	WAY-31
R. Hueting	Philips Research	WAG-12
B. Huizing	Philips Research	WAG-13
D. Klaassen	Philips Research	WAG-13

Full report

A. Aarts	Philips Research	WAG-13
W. Kloosterman	Philips Research	WAG-13
A. van de Ven	Eindhoven University of Technology	

©Philips Electronics N.V. 2000